# Estimation of effective cohesion using artificial neural networks based on index soil properties: a Singapore case

Yongmin Kim[a], Alfrendo Satyanaga[b], Harianto Rahardjo[c*], Homin Park[d], Aaron Wai Lun Sham[e]

[a]School of Engineering, University of Glasgow Singapore, Singapore.

[b]School of Civil and Environmental Engineering, Nazarbayev University, Kazakhstan

[c]School of Civil and Environmental Engineering, Nanyang Technological University, Singapore; [*]Corresponding author: *chrahardjo@ntu.edu.sg*

[d]Institute of Infocomm Research, Agency for Science, Technology and Research, Singapore

[e]Special Functions Group, Enforcement & Structural Inspection Department, Building and Construction Authority, Singapore

Abstract

This study presents a development of a multi-layer perceptron (MLP) model to spatially estimate and analyze the variability of effective cohesion for residual soils that are commonly associated with rainfall-induced slope failures in Singapore. A number of soil data were collected from the various construction sites, and a set of qualified Nanyang Technological University (NTU) data were utilized to determine a criterion for data selection. Four index properties (i.e., percentage of fines and coarse fractions, liquid and plastic limits) were used as training parameters to estimate the effective cohesion of residual soils from different geological formations. Ordinary kriging analyses were carried out to analyze the spatial distribution and variability of effective cohesion. As a result, the appropriate effective cohesions can be estimated using the MLP model with the incorporation of the selected values of measured effective cohesion as training data and four index soil properties as input data. In the combination of estimated and measured effective cohesions, the spatial analysis using Kriging

method can clearly differentiate the variations in effective cohesion with respect to the different geological formations.

Keywords: residual soil; effective cohesion; index properties; artificial neural networks

## 1. Introduction

Slope failures have become one of the most frequent geo-hazards all over the world. Rainfall-induced slope failure is a common problem in many tropical areas, such as Singapore during rainy seasons. These type of slope failures are commonly found in residual soils that were derived from various geological formations. (Rahardjo et al., 2012; 2016). Furthermore, rapid growth of regional economies has resulted in tremendous demand for hillside developments involving engineered and fill slopes. These failures can pose potential danger to infrastructures and public safety (Kim et al., 2018; Rahardjo et al., 2019a).

The geology of Singapore is closely related to the Malaysian geology. Located in the proximity of the tip of the South Malaysian Peninsula, the main North-North-West to South-South-East parallel belts are strongly defined in the Singapore realm. Thus, the Eastern and Central Belts of Malaysia continue to Singapore Island (Oliver and Gupta, 2017; Ip et al., 2021), predominant with the sandstones and mudstones. The geology of Singapore shows eight units but it consists mainly of three formations: 1) Jurong Formation (JF) which exhibits sedimentary rocks in the west; 2) Bukit Timah Granite (BTG) which exhibits igneous rocks of granite in the central and northwest; 3) Old Alluvium (OA) which exhibits semi-hardened alluvium in the east of Singapore (PWD, 1976). Fig. 1 shows a simplified geology map that outlines the distribution of the three major geological formations of Singapore.

Residual soil is the final product of the in-situ mechanical and chemical weathering of underlying rocks (Blight and Leong, 2012). The most important characteristic of residual soils is its reduced strength from the original rock's strength due to the destruction of the bonds and

the cementation of the material due to the weathering processes (Zhai et al., 2018). In addition, slopes covered with these residual soils in Singapore often have a problem during heavy rainfall events since the infiltration of rainwater into the unsaturated zone increases the pore-water pressure and subsequently decreases the shear strength (Fredlund and Rahardjo, 1993). As a result, rainfall-induced slope failures frequently happen in areas that are covered with residual soils (Rahardjo et al., 2013; 2014).

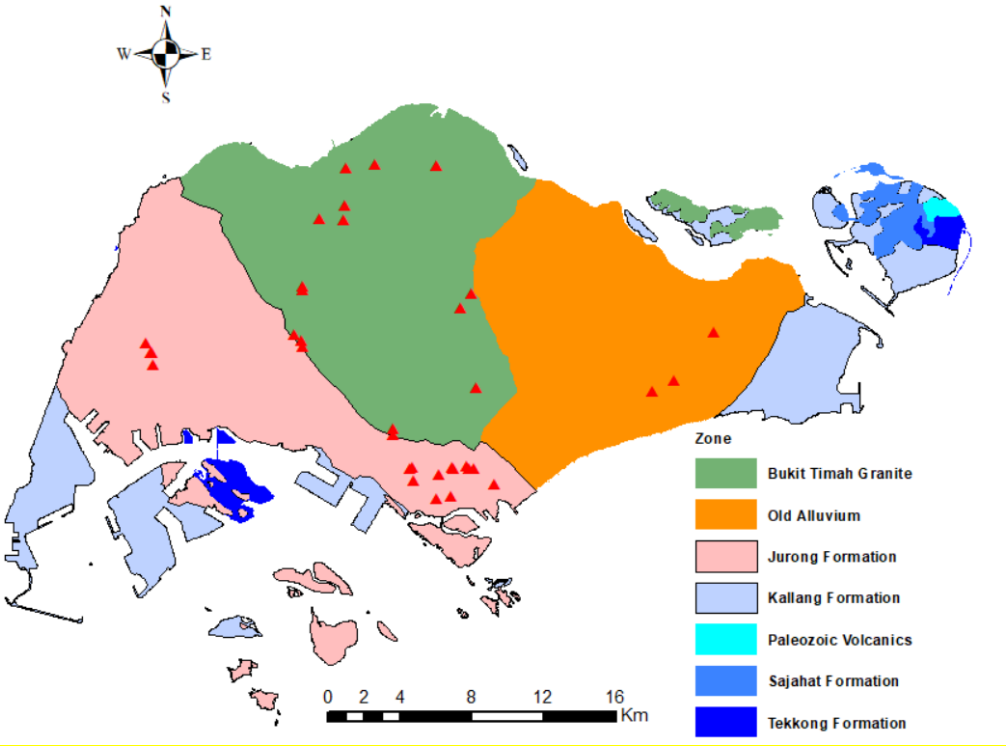


Fig. 1. Geological map of Singapore and locations of NTU database.

Shear strength properties of a soil are important parameters in determining stability of geotechnical structures. In particular, effective cohesion ($c'$) is one of the important shear strength parameters to evaluate slope stability. Therefore, theoretical equations to calculate factor of safety incorporates the term of $c'$. US Army Corps of Engineers (2003) observed that the factor of safety is significantly affected by $c'$. However, the weathering processes resulted in the change and the variation of $c'$ for residual soils in Singapore. Rahardjo et al. (2012) and Zhai et al. (2017) investigated the variability of residual soil properties with different soil depths and discussed that typical $c'$ of residual soils from Jurong Formation (JF), Bukit Timah

Granite (BTG), and Old Alluvium (OA) decreases with depth due to the decrease in the percentages of fine fractions. The mean values of $c'$ for residual soils vary from 8 kPa to 24 kPa over Singapore. Although the variability of $c'$ represented the characteristics of residual soils and the weathering processes in Singapore, a set of soil samples used has limited capabilities in representing the entire region due to its restricted sampling location coverage. Therefore, for the study on rainfall-induced slope failures, it is necessary to collect big data on soil properties to quantify the characteristics of $c'$ for residual soil with respect to the three different geological formations.

Recently, artificial neural network (ANN) models have drawn significant attention from the geotechnical engineering field. The ANN model can be applied to the analysis of geotechnical structures, e.g., shallow foundations (Kalinli et al., 2011) and landslides (Choi et al., 2012), and soil properties, e.g., shear strength of soils (Khanlari et al., 2012). Despite a growing interest in ANN models to deal with big geotechnical data, very few studies have considered soil properties that govern soil behavior because of the uncertainties in the variability of soil properties and difficulties in collecting soil samples. In addition, high-performance computing devices have made ANNs possible to have multi hidden layers and thousands of nodes. Such techniques with various hyperparameters have not been applied to past research works.

The main objective of this study is to spatially analyze the variability of effective cohesion for residual soils in Singapore. Soil data were collected from the various construction sites, and the qualified Nanyang Technological University (NTU) database was used to determine the upper and lower limits for data selection purposes. Index properties (i.e., percentage of fines and coarse fractions, liquid and plastic limits) were adopted as training data to estimate $c'$ using a multi-layer perceptron (MLP) model that can differentiate the variability

of $c'$ for residual soils from different geological formations. In addition, the spatial distributions of $c'$ were obtained by conducting ordinary kriging, and the variability of $c'$ was discussed.

## 2. Artificial neural networks (ANNs) for the estimation of effective cohesion

### *2.1 Introduction to ANNs*

Artificial neural networks (ANNs) are complex computing systems inspired by the biological neural networks resembling how neurons are tightly connected to form a layered network structure. Such systems learn to solve various tasks, including approximation, classification, and clustering, by thoroughly analyzing provided big data without exploiting prior-knowledge and task-specific rules (Luger, 2005).

There are three key advantages of ANNs as compared to conventional machine learning techniques. First, with sufficient training data, ANNs can learn and model latent relationships between inputs and outputs that are not obvious to human experts, which potentially leads to better performance. Second, ANNs can generalize its learned relationships to make accurate inference and prediction results in practice where unseen, yet from similar probabilistic distributions, data are often observed. Note that the learned characteristics (or features) are hidden behind the complex network structure. Therefore, ANNs are often denoted as a black-box system. Third, ANNs do not impose any restrictions on the input variable, which can quickly initiate the training process using the raw data instead of spending hours and days finding a set of feasible features that might represent the relationship between the inputs and outputs. In fact, with sufficient training data and carefully designed network architecture, ANNs demonstrated its significance over other conventional machine learning techniques in many domains (Shahin et al., 2001; Abiodun et al., 2018).

The use of ANN models has been found in the studies addressing issues in geotechnical structures and soil properties. For geotechnical structures, many researchers studied an ANN

model to predict bearing capacity of deep foundations (Goh, 1995; Chan et al., 1995; Lee and Lee, 1996). Settlement of shallow foundations was also inferred using an ANN model (Sivakugan et al., 1998; Shahin et al., 2000). Stability of slopes was evaluated by combining the fuzzy sets theory with ANNs (Ni et al., 1996). For soil properties, Ellis et al. (1995) proposed an ANN model to predict grain size distribution and stress history of sand. Cal (1995) developed an ANN model to generate a quantitative soil classification from index properties e.g., plastic index, liquid limit, and clay content. Romero and Pamukcu (1996) presented an ANN model to characterize shear modulus and granular materials. The application of ANNs to different aspects has increased in recent years. ANNs have been applied in predicting water quality (May and Sivakumar 2009), modeling of the rainfall-runoff process (Ju et al. 2009), forecasting of sewer overflow (Fernando et al. 2005) and river flow (Fernando and Shamseldin 2009), and predicting pore-water pressure in response to rainfall (Mustafa et al., 2012). Recently, ANNs are extended to multi-hidden layered architectures in multi-layer perceptron (MLP), which is one of the widely used ANN architectures resulting from developments of high-performance computing devices. MLP is computationally more efficient (e.g., faster training time, a smaller number of parameters, etc.) as compared to other predictive models (e.g., deep feedforward neural networks, convolutional neural networks, recurrent neural networks) that are not designed to address the soil data used in this study. Thus, MLP is suitable for analysis of scattered soil data.

### *2.2 MLP and Hyperparameters*

In this study, MLP was employed to estimate the effective cohesion for residual soils in Singapore. As illustrated in Fig. 2, a typical MLP architecture includes multiple layers of nodes, namely an input layer, a set of hidden layers, and an output layer. The number of nodes in each layer is determined as follows. First, the input layer equals to the number of input

variables (e.g., the number of soil properties used to predict the effective cohesion). Second, the number of hidden layers and the number of nodes in each hidden layer are iteratively determined in accordance with the data for training. Lastly, the output layer contains a single node to make estimations based on the input data. An empirical experiment was conducted to identify a suitable MLP design for this study, which includes two hidden layers, each containing one thousand nodes. It is noteworthy that increasing the depth of the network by adding more layers, which eventually leads to a deep feedforward neural network, decreased performance due to the overfitting issue. On the other hand, with a fixed number of hidden layers (e.g., two hidden layers) increasing the number of nodes, to a certain limit, improve the overall performance. This analysis suggests that the network must be shallow while the width is wide enough.

The initial inputs to the network are the borehole data $x = \{x_1, \dots, x_l, \dots, x_L\}$ that must be analyzed and learned to estimate the corresponding effective cohesion. Here, $L$ denotes the number of soil properties, and $l$ refers to the property index. Once $x$ is fed to the network, each node sequentially calculates the weighted sum of its inputs and transmits an output value determined by an activation function. As shown in Fig. 2, each node is fully connected with nodes from another layer by allowing the output of a node to become the input of the others. The activation function provides a differentiable transition in output values as input values change, allowing each node to decide whether to produce an output or not based on the input they received. There are several activation functions designed to serve different purposes (e.g., rectified linear unit, sigmoid, linear functions, etc.), and it is important to select a proper activation function to train the network (Luger, 2005). To effectively train the network, the rectified linear unit (ReLU) was employed while the output node exploited the linear activation function to make accuracy effective cohesion estimations. The advantages of using ReLU compared to other functions are 1) better gradient propagation which is necessary to update all

weights throughout the network, 2) computationally efficient by only using only addition and multiplication, and 3) sparse activation leading to better generalization (Nair et al., 2010). The ultimate output of the network $\hat{y}$ is made at the output layer, which tends to be erroneous during the early stages of training. The accuracy of $\hat{y}$ gradually improves as the network learns the latent relationship between the input data $x$ and the target (ground-truth) data $y$.

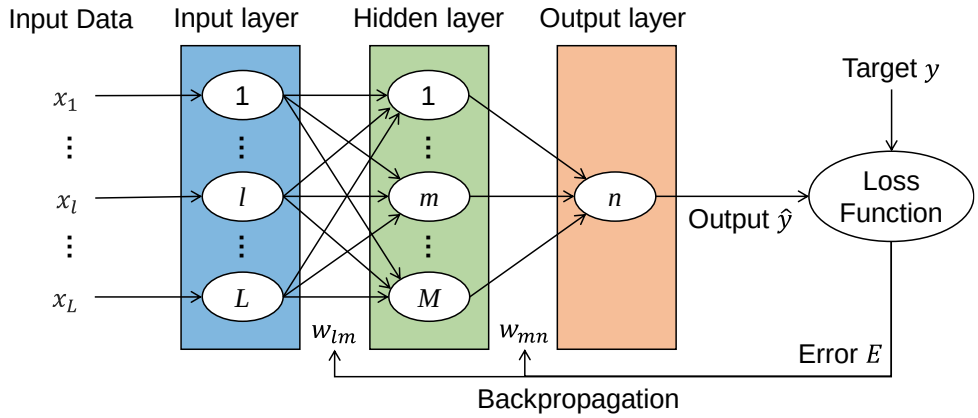


Fig. 2. Schematic diagram of a multi-layer perceptron.

The learning procedure involves adjusting the weights of the network to improve the accuracy of the estimation results. This is governed by three key factors, including loss function, learning rate, and backpropagation. To minimize the error, which leads to better performance, a loss function (e.g., root mean square error) quantifies the difference between the estimation result $\hat{y}$ and the ground-truth value $y$. The training process is determined to be completed when the error does not significantly decrease after updating the weights. In this study, the loss (error) is computed using root mean square error (RMSE) as follows:

$$RMSE = \sqrt{\sum_{t=1}^{T}(\hat{y}_a - y_a)^2 / N} \quad (1)$$

where $T$ is the number of training data instances while $t$ is the data instance index.

The backpropagation is a method to adjust each of the weights in the network in order to produce outputs closer to the target values, thereby minimizing the error. The derivation of

the backpropagation was performed by applying the chain rule to the error function partial derivative

$$\frac{\partial E}{\partial w_{ij}^k} = \frac{\partial E}{\partial a_j^k}\frac{\partial a_j^k}{\partial w_{ij}^k} \quad (2)$$

where $a_j^k$ is the activation of node $j$ in layer $k$ before it is passed to the nonlinear activation function to generate the output. The first term is often denoted as the error

$$\delta_j^k = \frac{\partial E}{\partial a_j^k} \quad (3)$$

while the second term is computed as:

$$\frac{\partial a_j^k}{\partial w_{ij}^k} = \frac{\partial}{\partial w_{ij}^k}\left(\sum_{l=0}^{r_{k-1}} w_{lj}^k o_l^{k-1}\right) = o_i^{k-1} \quad (4)$$

where $r_{k-1}$ is the number of nodes in layer $k-1$ and $o_i^{k-1}$ is the output of node $i$ in layer $k-1$. Thus, the partial derivative of the error $E$ with respect to a weight $w_{ij}^k$ is

$$\frac{\partial E}{\partial w_{ij}^k} = \delta_j^k o_i^{k-1} \quad (5)$$

which is a product of the error at node $j$ in layer $k$ and the output $o_i^{k-1}$ in layer $k-1$. Since the error $\delta_j^k$ depends on the values of error terms in the next layer $k+1$, the computation of the error terms will proceed backwards from the output layer down to the input layer, thus backpropagating the errors. In this study, Stochastic Gradient Descent (SGD) algorithm was exploited to train the model, which iteratively optimizes the network using an estimate of the gradient (calculated from a randomly selected subset of the data) instead of the actual gradient (calculated from the entire dataset).

Once the amount of adjustment needed for each weight is computed using SGD, the learning rate is applied to control the actual amount of adjustment made to the weights. A higher learning rate shortens the training time by making drastic changes to the weights but lowers overall accuracy due to the likelihood of finding a local minimum. On the other hand, a lower learning rate takes longer since we are making smaller changes to the weights but has

a higher chance of finding a global minimum (or a local minimum closer to that of global) yielding better performances. Each weight is thus updated as

$$\hat{w}_{ij}^{k} = w_{ij}^{k} - \eta \frac{\partial E}{\partial w_{ij}^{k}} \quad (6)$$

where $\eta$ is the learning rate. In this study, the learning rate was set to 0.000001.

*2.3 Detailed Training Procedure*

The training procedure used in this study can be summarized into five stages, as shown in Fig. 2, including 1) create a training dataset $X$ , 2) feedforward input data through MLP, 3) compute the loss, 4) calculate gradient, and 5) adjust the weights by backpropagation.

The very first step to creating a train and test dataset was to import raw data composed of five columns representing the % fine fraction, % coarse fraction, liquid limit (LL), plastic limit (PL), and $c'$. Once the raw data were loaded, the four index properties were used as the input data $x \in X$ while $c'$ was taken as the target data $y \in Y$. Lastly, $X$ and $Y$ were split into train and test sets where 75% of the data was used for training, while the other 25% was used for testing. Once the data was ready, the following steps were taken to train the MLP.

1. Randomly initialize the weights $W$
2. Feed the training data = {input $x$, target $y$}
3. Attain estimation value $\hat{y}$
4. Calculate the errors $E$ = RMSE($\hat{y}$, $y$)
5. Backpropagate the error $E$ by computing $\partial E/\partial w_{ij}^{k}$ using equations 2 to 5
6. Determine the actual adjustment needed for each weight using equation 6
7. Update the network weights
8. Repeat steps 2 to 7 until the required performance is met.

The early stopping of the training process was triggered if one of the followings was satisfied: 1) the loss (RMSE) is less than or equal to a predefined value or 2) the training takes longer than a specified number of epochs.

## 3. Methodology

### *3.1. Collection of soil data*

Two sets of soil data were collected in this study. First, residual soil samples were collected from 37 slopes which are located in the three different formations in Singapore, i.e., Jurong Formation (JF), Bukit Timah Granite (BTG), and Old Alluvium (OA), as shown in Fig. 1. A Mazier sampler was used, and the drillings of each borehole were carried out up to 6 m depth. All soil samples were waxed and stored inside a curing room with a constant water content ($w$) to maintain the natural condition. Index property tests were carried out to obtain grain-size distributions (ASTM D422-63, 2002) and Atterberg limits (ASTM D4318-00, 2002). For mechanical properties, consolidated undrained triaxial tests with pore-water pressure measurements on saturated soil specimens (ASTM D4767-04, 2002) and consolidated drained triaxial tests on unsaturated soil specimens (Satyanaga and Rahardjo, 2019) were carried out to obtain shear strength parameters of the soils. Table 1 summarizes the index and mechanical properties of residual soils, and hereafter called the NTU soil database.

Table 1. Summary of residual soil properties in Singapore (NTU soil database).

| No. | Geological formation | USCS* | % Coarse | % Fine | LL (%) | PL (%) | $c'$ (kPa) |
|---|---|---|---|---|---|---|---|
| 1 | BTG | MH | 22 | 78 | 52 | 34 | 9 |
| 2 | BTG | MH | 30 | 70 | 54 | 29 | 11 |
| 3 | BTG | SM | 58 | 42 | 56 | 38 | 5 |
| 4 | BTG | SC | 65 | 35 | 72 | 31 | 6 |
| 5 | BTG | SC | 66 | 34 | 48 | 37 | 6 |
| 6 | BTG | SM | 54 | 46 | 52 | 31 | 9 |
| 7 | BTG | SM | 61 | 39 | 108 | 47 | 7 |

| | | | | | | | |
|---|---|---|---|---|---|---|---|
| 8 | BTG | MH | 38 | 62 | 105 | 47 | 11 |
| 9 | BTG | MH | 5 | 95 | 72 | 45 | 13 |
| 10 | BTG | CH | 36 | 64 | 71 | 34 | 12 |
| 11 | BTG | MH | 42 | 58 | 61 | 36 | 7 |
| 12 | BTG | MH | 44 | 56 | 54 | 33 | 8 |
| 13 | JF | CL | 0 | 100 | 49 | 24 | 15 |
| 14 | JF | CL | 25 | 75 | N/A | N/A | 16 |
| 15 | JF | CL | 14 | 86 | 29 | 18 | 8 |
| 16 | JF | SC | 30 | 70 | N/A | N/A | 6 |
| 17 | JF | MH | 20 | 80 | 45 | 24 | 6 |
| 18 | JF | MH | 37 | 63 | 62 | 36 | 9 |
| 19 | JF | CH | 18 | 82 | N/A | N/A | 8 |
| 30 | JF | CL | 3 | 97 | 39 | 19 | 14 |
| 21 | JF | CL | 2 | 98 | 38 | 18 | 13 |
| 22 | JF | SC | 87 | 13 | 47 | 14 | 4 |
| 23 | JF | CL | 24 | 76 | 36 | 17 | 6 |
| 24 | JF | MH | 30 | 70 | 32 | 20 | 7 |
| 25 | JF | N/A | 25 | 75 | N/A | N/A | 8 |
| 26 | JF | CL | 14 | 86 | 39 | 29 | 9 |
| 227 | JF | CL | 23 | 77 | 47 | 26 | 7 |
| 28 | JF | MH | 27 | 73 | 55 | 33 | 10 |
| 29 | JF | ML | 44 | 56 | 42 | 27 | 6 |
| 30 | JF | CL | 23 | 77 | 47 | 26 | 20 |
| 31 | JF | CL | 15 | 85 | 34 | 20.5 | 20 |
| 32 | JF | CL | 13 | 87 | 39 | 24 | 13 |
| 33 | OA | SC | 70 | 30 | 47 | 23 | 3 |
| 34 | OA | CH | 51 | 49 | 42 | 19 | 5 |
| 35 | OA | SC | 80 | 20 | 34 | 18 | 6 |
| 36 | OA | SP | 96.8 | 3.2 | N/A | N/A | 2 |
| 37 | OA | SM | 68 | 32 | 72 | 28 | 2 |
| 38 | OA | CL | 75 | 25 | 60 | 36 | 9 |

*: Unified Soil Classification System

Second, borehole data obtained from the Integrated Land Information Service (INLIS) portal with bore logs information from the various construction sites were collected in this study. In total, 1870 bore logs were analyzed consisting of 23,936 boreholes across Singapore, ranging from 1990 to 2014. Typical information found in the bore logs are the results of the index properties test, standard penetration test, soil classification, grain-size distribution test, triaxial test, piezometer reading, and others. In this study, soil information up to 6 m depth was retrieved for the study on rainfall-induced slope failure because shallow failures in residual soils are the predominant mode of rainfall-induced slope failures in Singapore (Rahardjo et al.

2007). Table 2 summarizes the number of results of the various relevant soil properties used in this study. The total number of available data sets including index properties and effective cohesion from JF, BTG, and OA areas are 64, 332, and 209 sets, respectively.

Table 2 Summary of the total number of soil information up to 6 m depth

| Information | Total number |
|---|---|
| Construction project | 1870 |
| Borehole | 23936 |
| Unit weight | 23694 |
| Grain-size distribution | 7822 |
| Atterberg limits | 3613 |
| Effective cohesion | 2093 |
| Available data in Jurong Formation | 64 |
| Available data in Bukit Timah Granite | 332 |
| Available data in Old Alluvium | 209 |

*2.2 Selection of qualified soil data*

In general, the soil properties from site investigations in Singapore include natural water content, specific weight, Atterberg limits, grain size distributions, saturated permeability, effective cohesion, effective internal friction angle, etc. Among them, index properties, i.e., LL, PL, percentages of fine and coarse fractions, were selected as input parameters in the prediction because the index properties can be easily obtained from the simple laboratory tests. In addition, the effective cohesion ($c'$) exhibits linear relationships with the percentage of fine fractions. Fig. 3 shows the $c'$ distribution with the percentage of fine fraction from the NTU soil database. The $c'$ tended to increase with an increase in the percentage of fine fractions.

The upper and lower limits of the $c'$ distributions were calculated using a confidence interval approach (Kool and Parker, 1988; Satyanaga et al., 2017; Rahardjo et al., 2019b). Confidence limits of the parameters could be determined from individual parameter variance as approximated using t-statistics. In this study, two-sided confidence limits with a 99 % level of confidence and t-statistics tool were adopted for the determination of confidence limits of

the $c'$ distribution with respect to the percentage of fine fraction for residual soil in Singapore. For the selection of the qualified soil data, upper and lower limits with a 99 % level of confidence were applied to the collected borehole data. Fig. 4 shows the selected training data of each rock formation.

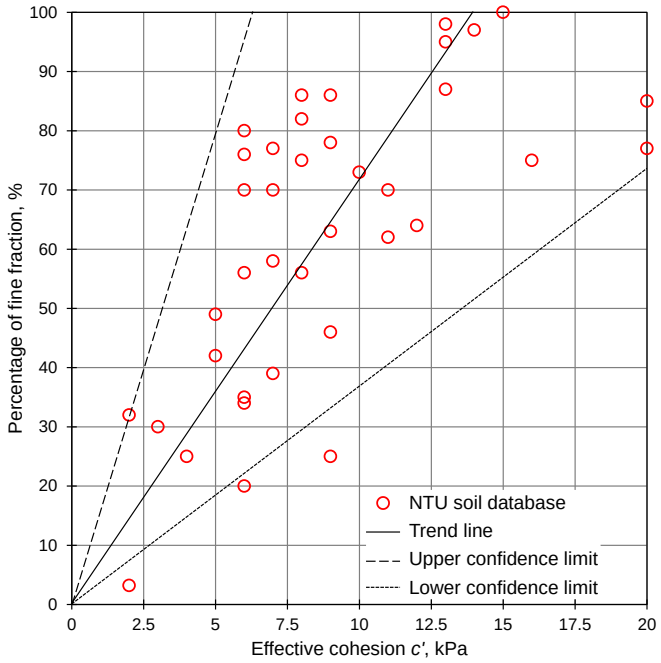


Fig. 3. Upper and lower limits of the NTU database on the relationship between effective cohesion and percentage of fine fraction

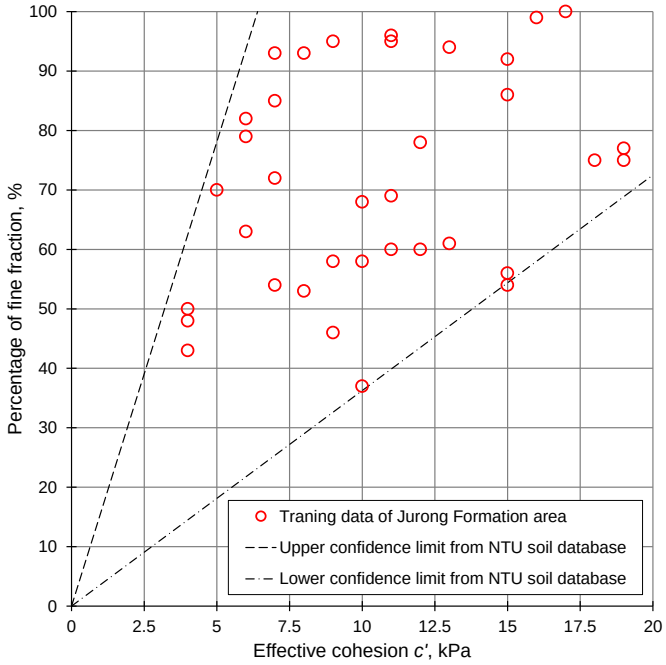


(a) Jurong Formation area

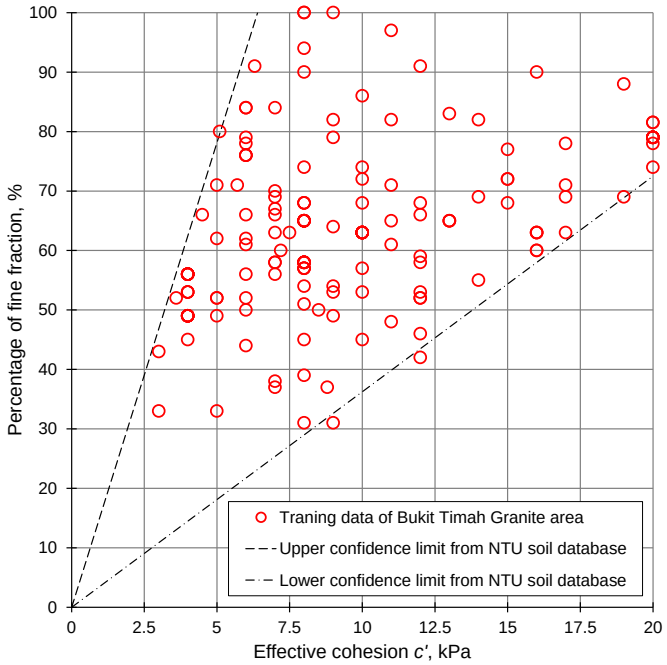


(b) Bukit Timah Granite area

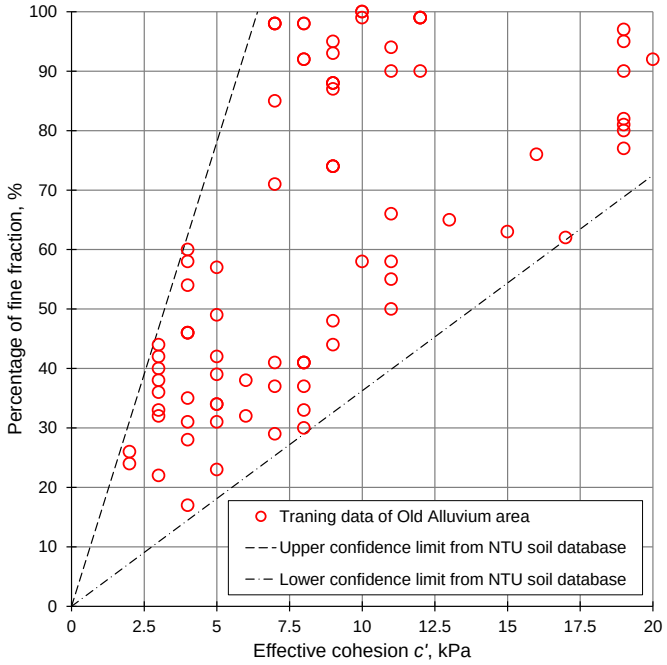


(c) Old Alluvium area

Fig. 4. Selected training data of each geological formation.

*3.3 Spatial distribution of effective cohesion*

Soil shear strength parameters such as effective cohesion (*c'*) from site investigations exist discrete measurement points in space. Therefore, digital soil mapping is capable of

297 characterizing the properties of residual soil at all locations. It requires statistical methods such
298 as kriging to interpolate the values of a random field at an unobserved location from
299 observations of its value at nearby locations. Previous studies provide various examples of
300 kriging used to develop slope susceptibility maps. Roslee et al. (2012) and Jibson et al. (2000)
301 used simple kriging when developing landslide susceptibility analyses. Ordinary kriging has
302 also been used to develop landslide prediction and to produce rainfall maps in Taiwan (Chiang
303 and Chang, 2009; Ip et al., 2020; 2019). They found that ordinary kriging predicted the closest
304 to radar rainfall estimates and performed better in predicting both landslide-prone and stable
305 areas.

306 In this study, ordinary kriging was conducted to interpolate the values of effective
307 cohesion over Singapore. Ordinary kriging is a form of kriging that assumes the underlying
308 random process to be intrinsically stationary with a constant mean over a local area, and the
309 variation in the regionalized variable depends only on separation in distance and direction
310 between points and not on absolute position (Goovaerts, 1997). The kriging estimate is a linear
311 weighted sum of observations from the surrounding area:

312 $$\hat{Z}(\boldsymbol{x_0}) = \sum_{i=1}^{N} \lambda_i z(\boldsymbol{x_i}) \quad (7)$$

313 where $\hat{Z}(\boldsymbol{x_0})$ is the estimated soil property by ordinary kriging, $N$ is the number of
314 observations, $\lambda_i$ is the weights, $z(\boldsymbol{x_i})$ is the observed soil parameter. The ordinary kriging
315 weights are chosen such that the kriging variance is minimized, and the estimate is unbiased
316 through Eq. 8 and 9:

317 $$\sum_{i=1}^{N} \lambda_i \gamma(\boldsymbol{x_i}, \boldsymbol{x_j}) + \psi(\boldsymbol{x_o}) = \gamma(\boldsymbol{x_o}, \boldsymbol{x_j}) \text{ for all j} \quad (8)$$

318 $$\sum_{i=1}^{N} \lambda_i = 1 \quad (9)$$

319 where $\psi(\boldsymbol{x_o})$ is the Lagrange multiplier, $\gamma(\boldsymbol{x_i}, \boldsymbol{x_j})$ is the semivariance between observation
320 locations and $\gamma(\boldsymbol{x_o}, \boldsymbol{x_j})$ is the semivariance between the estimation and the observation
321 locations.

## 4. Results and discussion

### *1) Validation*

A total number of complete data sets for residual soils from JF, BTG, and OA used for the MLP training was 37, 85, and 185 sets, respectively. A 25 % of the training data was used for validation at each geological formation, as explained in Section 2.3. Fig. 5 shows the relationship between estimated and measured effective cohesion within each area, and the corresponding loss associated with the predictions in JF, BTG, and OA areas was 5.4, 5.1, and 2.8 %, respectively. The results confirmed the fact that the developed ANN model and hyperparameters were appropriate to estimate the effective cohesion of residual soils based on index soil properties.

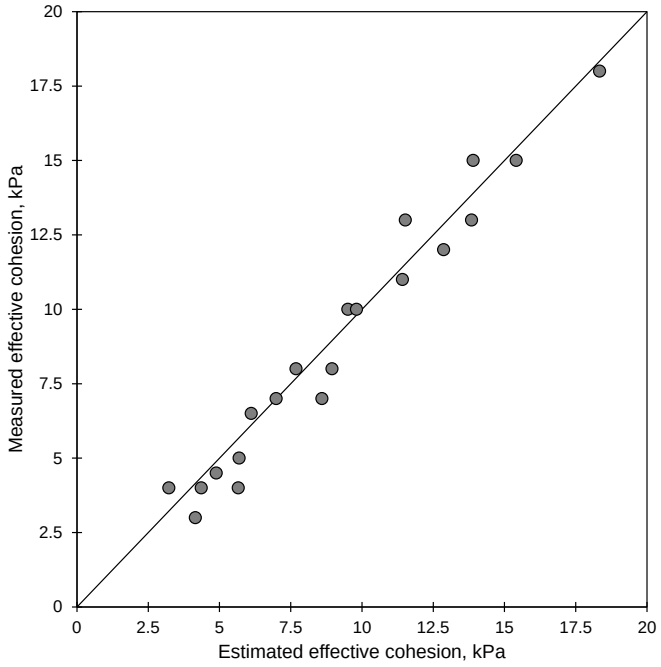


(a) Jurong Formation (JF) area

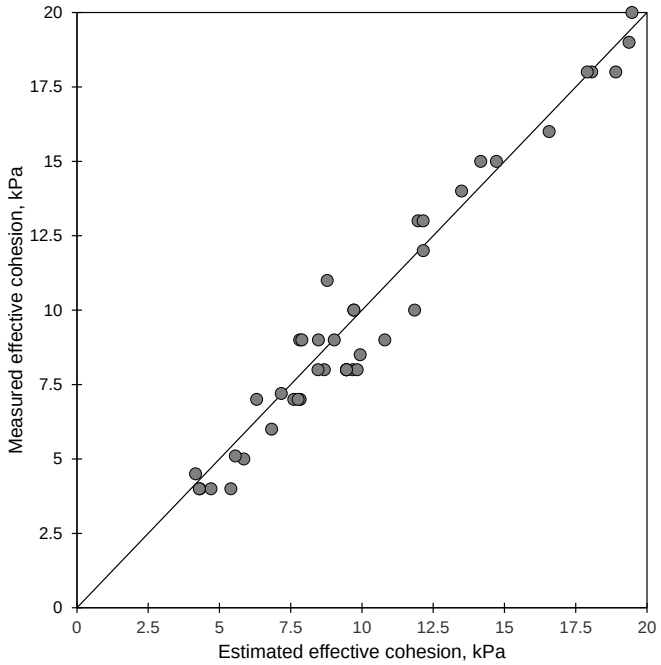


334

335 (b) Bukit Timah Granite (BTG) area

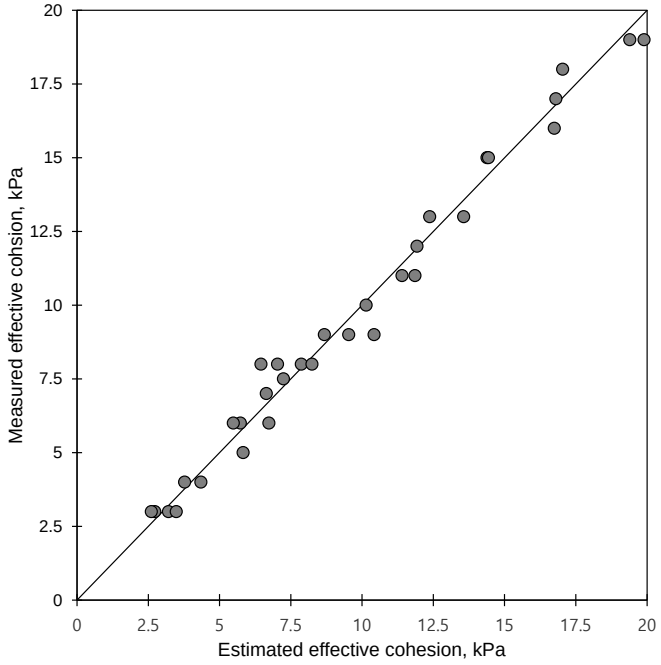


336

337 (c) Old Alluvium (OA) area

338 Fig. 5. Comparisons between predicted and measured effective cohesions.

339

340

341

342 *2) Results of c' estimation*

343 Effective cohesions of residual soils from JF, BTG, and OA areas were estimated using
344 the MLP model based on the index properties (i.e., grain size distributions and Atterberg limits).
345 The combination of the MLP architecture and the learning rate used in the training produced
346 accurate results with errors approximately up to 5 %. As expected, the estimated values of
347 effective cohesion ranged between upper and lower boundaries, as depicted in Fig. 6 because
348 the training data were selected by following the same upper and lower boundaries.
349 Consequently, the estimated effective cohesions using the MLP model were found to be
350 appropriate. Some effective cohesions exhibited outer boundaries due to numerical errors, but
351 the values are still in a reasonable range. A total number of the estimated *c'* of residual soils
352 from JF, BTG, and OA areas was 244, 1592, and 795, respectively. Table 3 summarizes the
353 number of data sets used for the *c'* estimation. Note that the terms of available data and training
354 data in Table 3 indicate the total number of collected data over Singapore and the selected data
355 by upper and lower confident limits for MLP training, respectively.

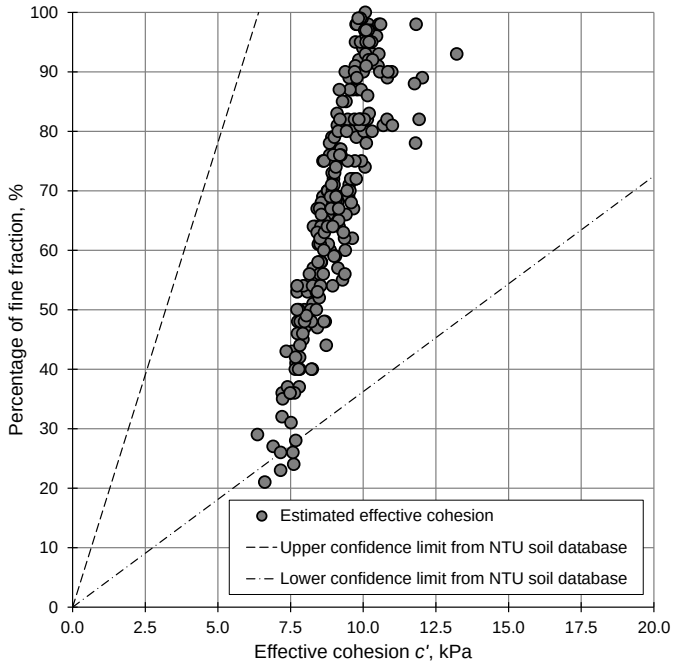


356

357 (a) Jurong Formation (JF) area

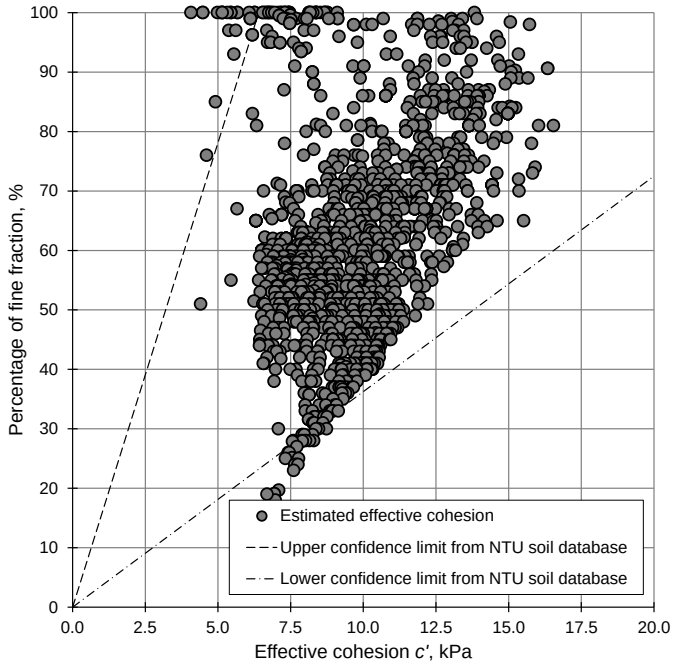


358

359 (b) Bukit Timah Granite (BTG) area

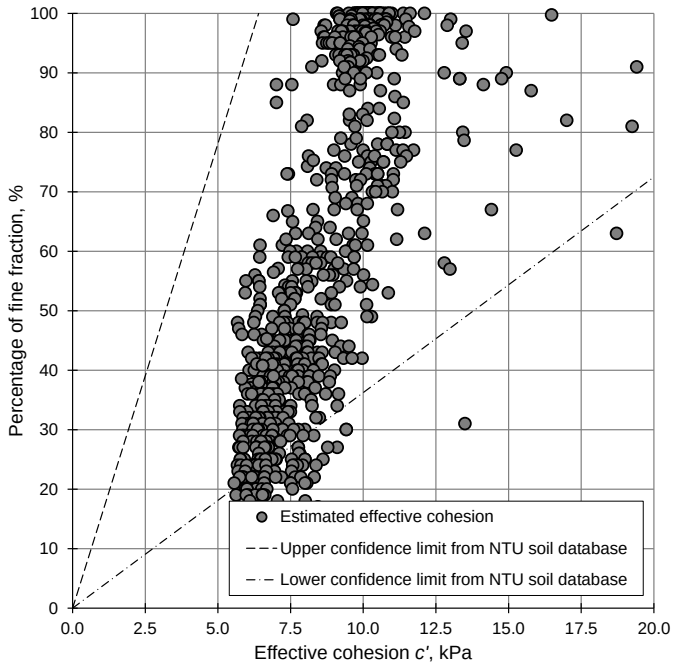


360

361 (c) Old Alluvium (OA) area

362 Fig. 6. Relationships between predicted effective cohesion and percentage of fine fraction

363

364

365

Table 3 Total number of data used in the estimation.

| Formation | Available data[a] | Training data[b] | Estimated data[c] | Total (a+c) |
|---|---|---|---|---|
| JF | 64 | 37 | 244 | 308 |
| BTG | 332 | 185 | 1529 | 1861 |
| OA | 209 | 85 | 795 | 1004 |

*3) Spatial distribution of c'*

The spatial distributions of *c'* were estimated utilizing an ordinary kriging method based on available data from JF (64 points), BTG (332 points), and OA (209 points), which did not include the results of *c'* estimation from the MLP model, as shown in Fig. 6. The variances with distance from the spatial distribution of *c'* for JF, BTG, and OA areas are presented in Fig. 7a, 7b, and 7c, respectively. It can be seen that the $R^2$ of the estimated data from the Kriging analysis is quite low (between 0.5 – 0.6). Hence, the spatial distribution of *c'* is not comparable with the measured *c'* data. In addition, the variances of BTG and OA areas indicated a high uncertainty in the estimation of *c'* using the kriging analysis.

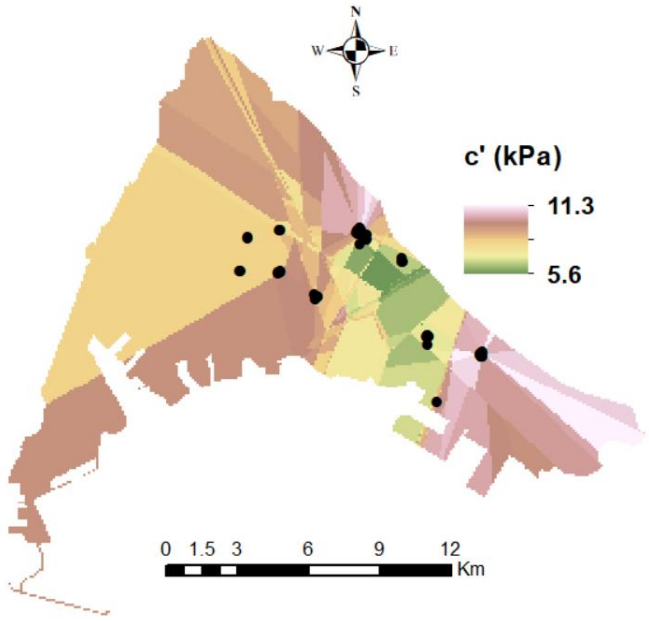


(a) Jurong Formation (JF) area

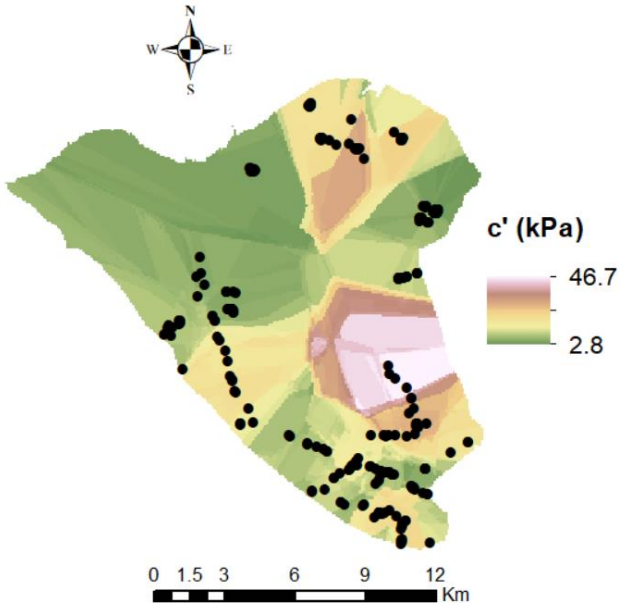


(b) Bukit Timah Granite (BTG) area

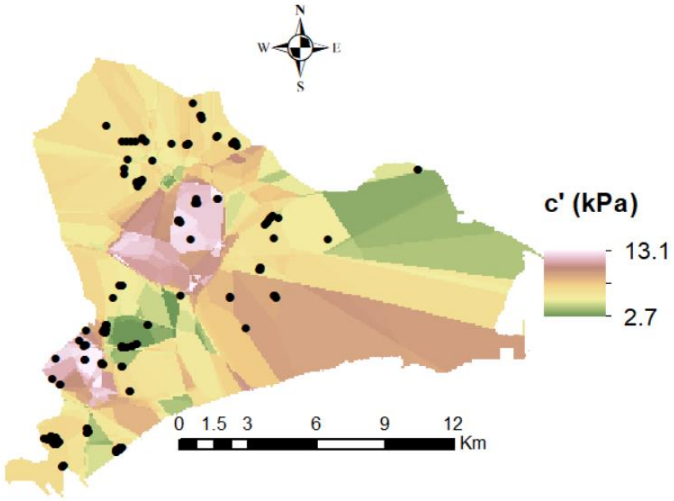


(c) Old Alluvium (OA) area

Fig 6. Spatial distribution of effective cohesion before the *c'* estimation

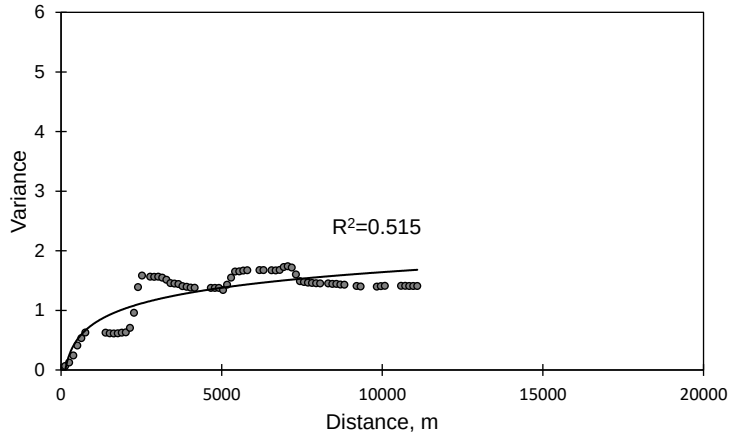


384

385 (a) Jurong Formation (JF) area

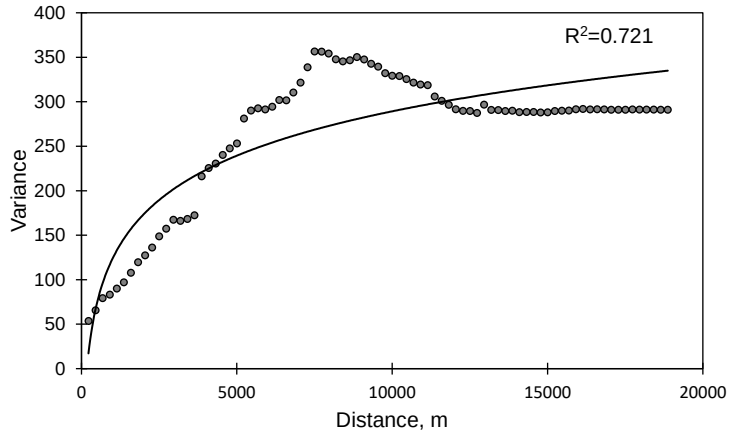


386

387 (b) Bukit Timah Granite (BTG) area

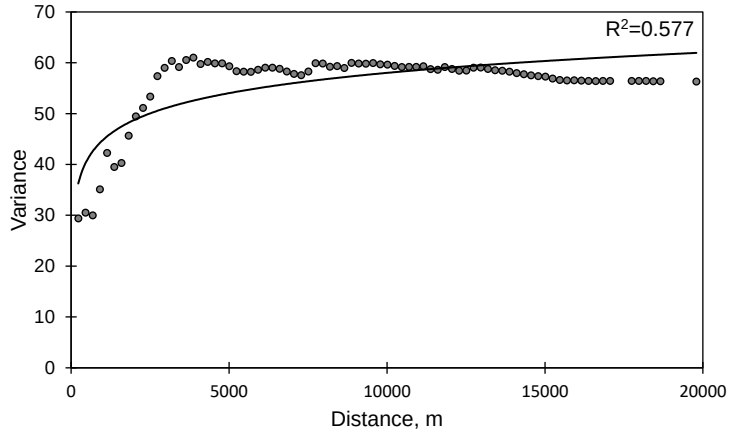


388

389 (c) Old Alluvium (OA) area

390 Fig. 7. Variances with distance from spatial distribution of $c'$ without MLP results

The spatial distributions of *c'* were estimated utilizing ordinary kriging methods based on total data from JF (308 points), BTG (1861 points), and OA (1004 points), which have included the results of *c'* estimation from the MLP model, as shown in Fig. 8. The variances with distance from the spatial distribution of *c'* for JF, BTG, and OA are presented in Fig. 9a, 9b, and 9c, respectively. It can be seen that the $R^2$ of the estimated data from the Kriging analysis is close to 0.9 indicating a good agreement between the estimated and measured *c'* data.

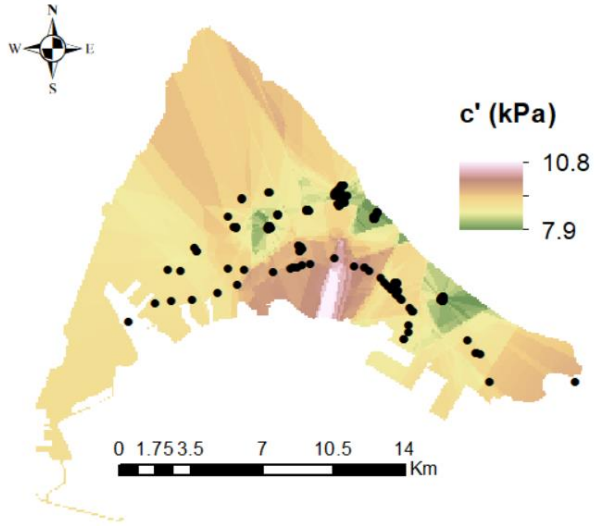


(a) Jurong Formation (JF) area

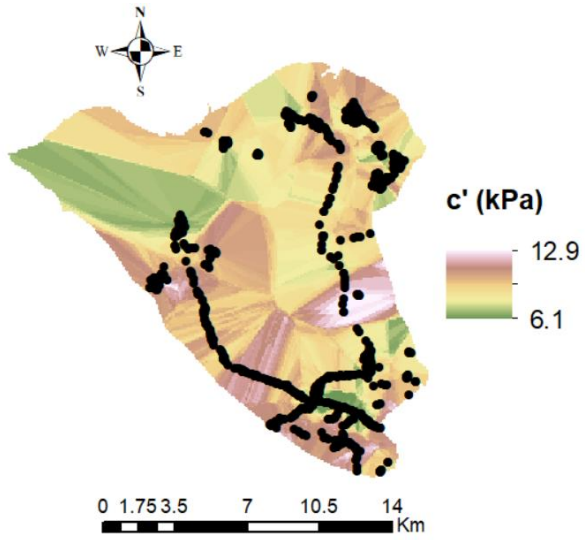


(b) Bukit Timah Granite (BTG) area

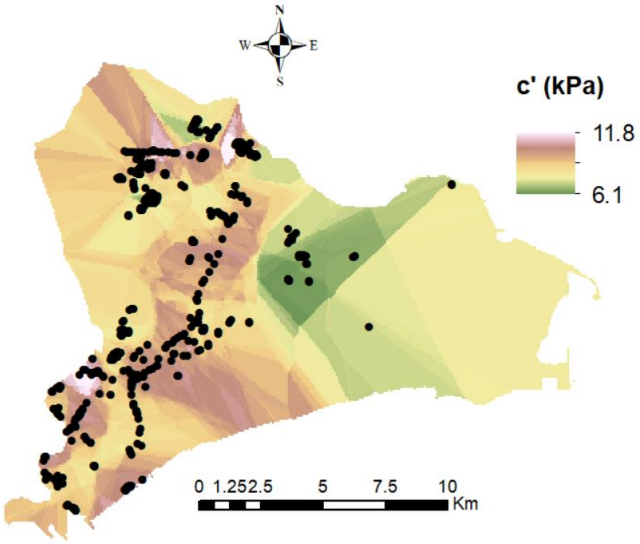


402

403 (c) Old Alluvium (OA) area

404 Fig 8. Spatial distribution of effective cohesion after the *c*' estimation.

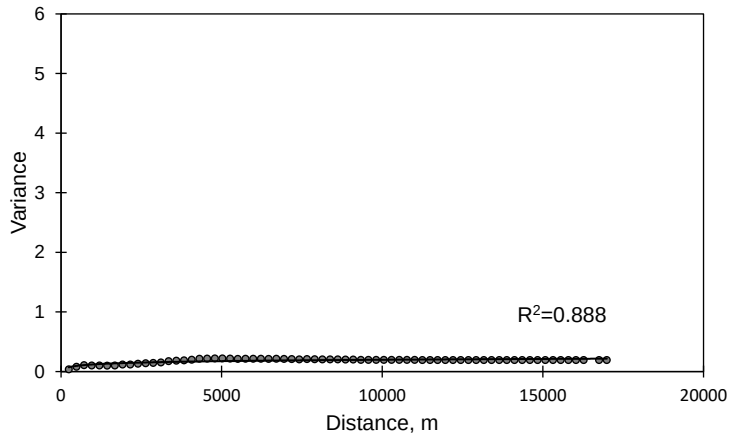


405

406 (a) Jurong formation area

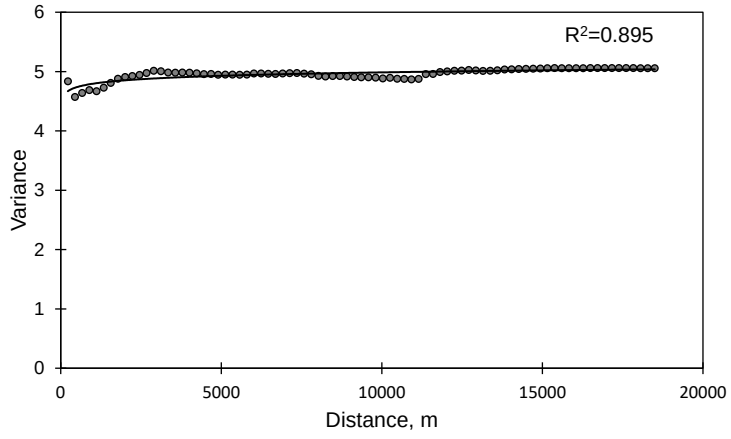


407

408 (b) Bukit Timah Granite areas

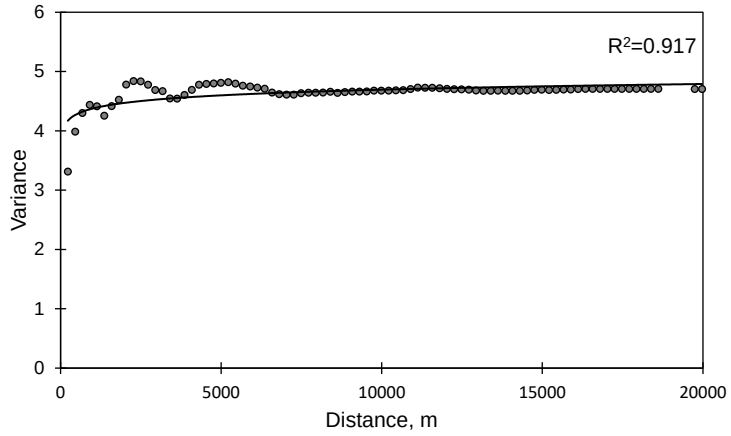


409

410 (c) Old Alluvium area

411 Fig. 9. Variances with distance from spatial distribution of *c*' with MLP results

412

413 *4) Variations of c' with respect to geological formations.*

414 The variations of *c*' before and after the MLP estimation are plotted to evaluate the
415 relevance of the *c*' data after kriging analyses. Figs 10-12 show that the ranges of the measured
416 *c*' are completely different from those of the estimated *c*' based on Kriging analyses without
417 MLP results. However, the ranges of the measured *c*' are similar to those of the estimated *c*'
418 based on Kriging analyses after MLP analyses were performed. The ranges of the measured *c*'
419 for the JF area before and after MLP analyses are between 0.0-19.0 kPa and 6.1-10.1 kPa,
420 respectively. The ranges of the measured *c*' for the BTG area before and after MLP analyses
421 are between 0.0-65.0 kPa and 4.0-16.5 kPa, respectively. The ranges of the measured *c*' for the
422 OA area before and after MLP analyses are between 0.0-30.0 kPa and 5.5-22.4 kPa,
423 respectively. It can be seen that the estimation from the MLP model is important to ensure the
424 boundary of the measured *c*' is reasonable prior to Kriging analyses. Upon Kriging analyses,
425 the ranges of the estimated *c*' are narrower as compared to those of the measured *c*' for all soil
426 s from the tree formations. It is also found that higher *c*' was obtained in JF as compared to
427 BTG. Similar trends concerning the ranges of *c*' were reported previously by Rahardjo et al.

(2004) in their experimental study. In addition, higher *c'* was obtained in OA as compared to BTG in this study. The ranges of *c'* predicted in BTG and OA are relatively similar to those presented in the literature of 4-17 kPa and 5-23 kPa, respectively (Rahardjo et al., 2012). Overall, the MLP is capable in predicting accurate values of *c'* for residual soils in Singapore and clearly differentiating *c'* values with respect to the different geological formations.

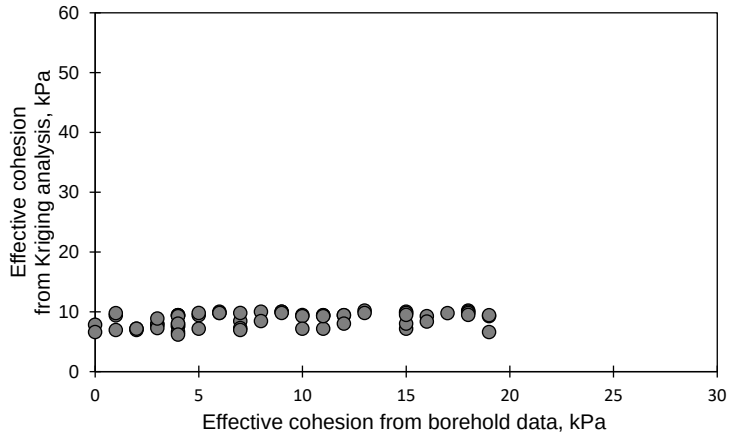


(a) without MLP results

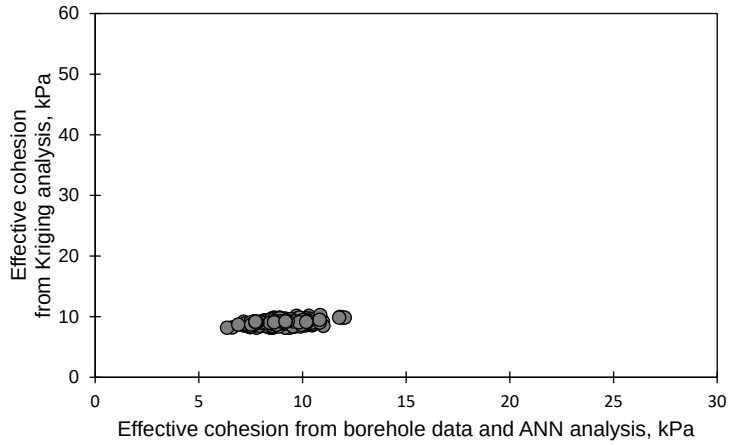


(b) with MLP results

Fig. 10. Comparisons of effective cohesion obtained from kriging analyses and borehole data (a) without MLP results; (b) with MLP results for Jurong Formation area.

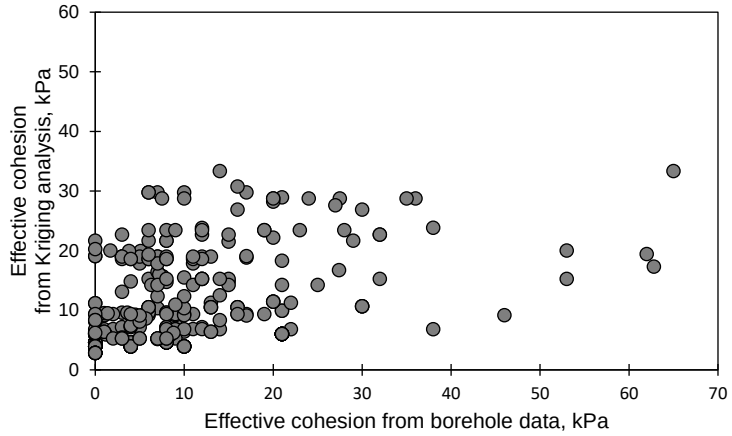


439

440 (a) without MLP results

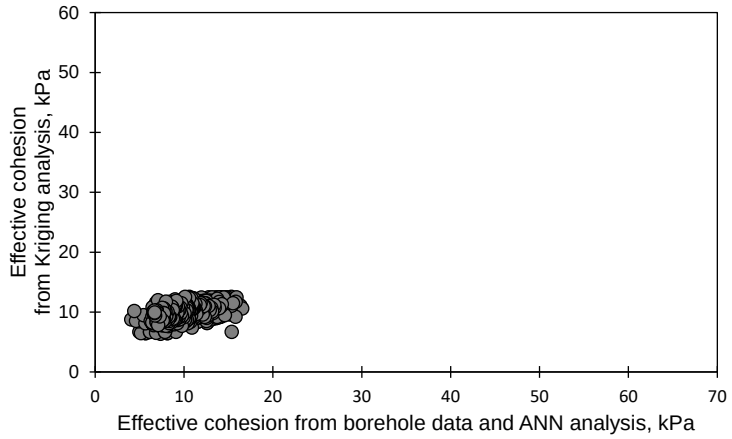


441

442 (b) with MLP results

443 Fig. 11. Comparisons of effective cohesion obtained from kriging analyses and borehole data

444 (a) without MLP results; (b) with MLP results for Bukit Timah Granite area.

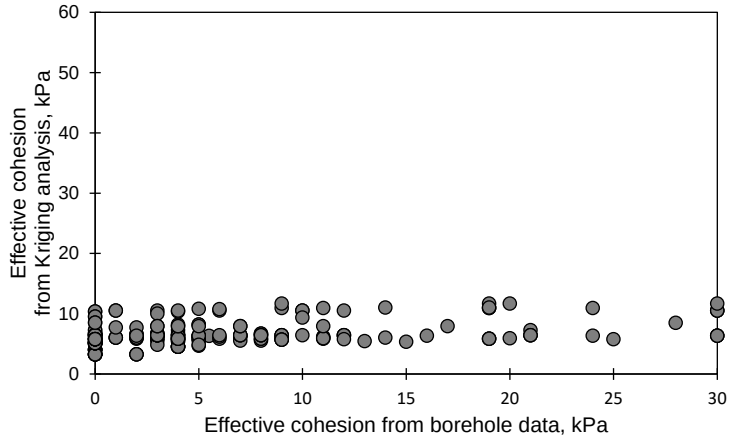


445

446 (a) without MLP results

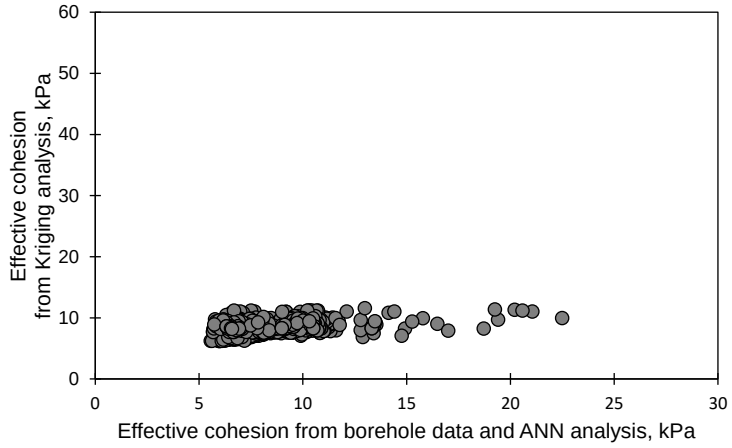


(b) with MLP results

Fig. 12. Comparisons of effective cohesion estimated from kriging analyses and borehole data (a) without MLP results; (b) with MLP results for Old Alluvium area.

## 5. Conclusions

A multi-layer perceptron model (MLP) was successfully developed to estimate effective cohesion of residual soils in Singapore. The appropriate neural network hyperparameters capable of relating between effective cohesion and index properties of residual soils i.e., percentage of fine and coarse fraction, liquid and plastic limits were presented. Determination of effective cohesion in a regional area using laboratory testing or empirical equations is difficult to conduct. However, the estimation of effective cohesion using the MLP model played a role to differentiate variations in effective cohesion with respect to soil properties from different geological formations when conducting spatial distribution analyses. The estimation results showed good agreement with the measured effective cohesions. The practical implementation of the MLP model associated with the qualified training data was to determine confident interval limits of effective cohesion distributions with respect to the percentage of fine fractions for residual soils in Singapore. This framework offers a valuable

basis for estimating effective cohesion in a regional area where the shear strength parameter is urgently needed for geotechnical engineering problems.

Acknowledgment

The authors would like to acknowledge the funding support from Building Construction Authority and the sharing of the data from Singapore Land Authority, who are the collaborator of the project on The Development of Slope Management and Susceptibility Geographical Information System.

References

Abiodun, O.I., Jantan, A., Omolara, A.E., Dada, K.V., Mohamed, A., Arshad, H., 2018. State-of-the-art in artificial neural network applications: A survey. Heliyon 4 (11), e00938.

ASTM D422-63, 2002. Standard Test Method for Particle Size Analysis of Soils.

ASTM D4318–00, 2000. Standard Test Methods for Liquid Limit, Plastic Limit, and Plasticity Index of Soils.

ASTM D4767-04, 2004. Standard test method for consolidated undrained triaxial compression test for cohesive soils.

Blight, G.E., Leong, E.C., 2012. Mechanics of residual soils. CRC Press.

Cal, Y., 1995. Soil classification by neural-network. Advances in Engineering Software, 22 (2), 95-97.

Chan, W.T., Chow, Y.K., Liu, L.F., 1995. Neural network: An alternative to pile driving formulas. Computers and Geotechnics, 17, 135-156.

Chiang S.H., Chang K.T., 2009. Application of radar data to modeling rainfall-induced landslides. Geomorphology, 103, 299–309.

Choi J., Oh, H.J., Lee, H.J., Lee, C., Lee, S., 2012. Combining landslide susceptibility maps obtained from frequency ratio, logistic regression, and artificial neural network models using ASTER images and GIS. Engineering Geology, 124 (4), 12-23.

Ellis, G.W., Yao, C., Zhao, R., Penumadu, D., 1995. Stress-strain modelling of sands using artificial neural networks. J. Geotech. Engrg., ASCE, 121 (5), 429-435.

Fernando, D.A.K., Shamseldin, A., 2009. Investigation of internal functioning of the radial basis function neural network river flow forecasting models. J. Hydrol. Eng., 14 (3), 286–292.

Fernando, D.A.K., Zhang, X., Kinley, P.F., 2005. Combined sewer overflow forecasting with feed-forward back-propagation artificial neural network. Int. J. Appl. Sci. Eng. Technol. 4, 212–217.

Fredlund, D.G., Rahardjo, H., 1993. Soil Mechanics for Unsaturated Soils. John Wiley & Sons, Inc., New York.

Goh, A.T.C., 1995. Empirical design in geotechnics using neural networks. Geotechnique, 45 (4), 709-714.

Goovaerts, P. 1997. Geostatistics for Natural Resources Evaluation. New York: Oxford University Press.

Ip., C.Y., Satyanaga, A. and Rahardjo, H. 2021. Spatial variation of shear strength properties incorporating auxiliary variables. Catena, May, Vol 200, 105196

Ip, C.Y., Rahardjo, H., Satyanaga, A. 2020. Three-dimensional slope stability analysis incorporating unsaturated soil properties in Singapore, Georisk: Assessment and Management of Risk for Engineered Systems and Geohazards, DOI: 10.1080/17499518.2020.1737880

Ip., C.Y., Rahardjo, H., Satyanaga, A. 2019. Spatial Variations of Air-entry Value for Residual Soils in Singapore. Catena, 174, pp. 259-268

514 Jibson, R.W., Harp, E.L., Michael, J.A., 1998. A method for producing digital probabilistic
515 seismic landslide hazard maps. Engineering Geology, 58 (3-4), 271-289.
516 Ju, Q., Yu, Z., Hao, Z., Ou, G., Zhao, J., Liu, D., 2009. Division based rainfall-runoff
517 simulations with BP neural networks and Xinanjiang model. Neurocomputing, 72 (13–
518 15), 2873–2883.
519 Kalinli, A., Acar, M.C., Gunduz, Z., 2011. New approaches to determine the ultimate bearing
520 capacity of shallow foundations based on artificial neural networks and ant colony
521 optimization. Engineering Geology, 117 (1-2), 29-38.
522 Khanlari, G.R., Heidari, M., Momeni, A.A., Abdilor, Y., 2012. Prediction of shear strength
523 parameters of soils using artificial neural networks and multivariate regression methods.
524 Engineering Geology, 131-132, 11-18.
525 Kim J., Hwang, W., Kim, Y., 2018. Effects of hysteresis on hydro-mechanical behavior of
526 unsaturated soil. Engineering Geology, 245, 1-9.
527 Kool, J.B., Parker, J.C., 1988. Analysis of the inverse problem for transient flow. Water
528 Resources Research, 24, 817–830.
529 Lee, I.M., and Lee, J.H., 1996. Prediction of pile bearing capacity using artificial neural
530 networks. Computers and Geotechnics, 18 (3), 189-200.
531 Luger, G.F., 2005. Artificial intelligence: structures and strategies for complex problem solving.
532 Pearson education.
533 May, D.B., Sivakumar, M., 2009. Prediction of urban storm water quality using artificial neural
534 networks. Environ. Model. Software, 24 (2), 296–302.
535 Mustafa, M.R., Rezaur, R.B., Rahardjo, H., Isa, M.H., 2011. Prediction of pore-water pressure
536 using radial basis function neural network. Eng. Geol., 135–136, 40–47.
537 Nair, V., Geoffrey E.H., 2010. Rectified linear units improve restricted boltzmann machines.
538 Proceedings of the 27th international conference on machine learning (ICML-10). 2010.

539 Ni, S.H., Lu, P.C., Juang, C.H., 1996. A fuzzy neural network approach to evaluation of slope
540 failure potential." J. Microcomputers in Civil Engineering, 11, 59-66.
541 Oliver, G.J.H., Gupta, A., 2017. In: Tan, Hugh T.W. (Ed.), A Field Guide to the Geology of
542 Singapore. Lee Kong Chian Natural History Museum, Singapore ISBN 978-981-09-
543 5714-8.
544 PWD, 1976. Geology of the Republic of Singapore. PublicWorks Department, Singapore.
545 Rahardjo, H., Kim, Y., Satyanaga, A., 2019a. Role of unsaturated soil mechanics in
546 geotechnical engineering, International Journal of Geo-Engineering 10 (1), 1-23.
547 Rahardjo, H., Satyanaga, A., Mohamed, H., Ip., C.Y., Rishi, S.S. 2019b. Comparison of Soil-
548 Water Characteristic Curves from Conventional Testing and Combination of Small-
549 Scale Centrifuge and Dew Point Methods. Journal of Geotechnical and Geological
550 Engineering, 37 (2), pp. 659-672.
551 Rahardjo, H., Satyanaga, A., Leong, E.C. 2016. Effects of rainfall characteristics on the
552 stability of tropical residual soil slope. Proceedings of E-UNSAT 2016, E3S Web of
553 conferences 9, Sep 2016, 15004, 1-6
554 Rahardjo, H., Satyanaga, A., Leong, E.C., Wang, J.-Y. 2014. Comprehensive Instrumentation
555 for Real Time Monitoring of Flux Boundary Conditions in Slope. Procedia Earth and
556 Planetary Science, 9, 23-43
557 Rahardjo, H., Satyanaga, A., Leong, E.C., 2013. Effects of Flux Boundary Conditions on Pore-
558 water Pressure Distribution in Slope. Engineering Geology, 165, 133-142.
559 Rahardjo, H., Satyanaga, A., Leong, E.C., Ng, Y.S., Pang, H.T.C., 2012. Variability of residual
560 soil properties. Engineering Geology, 141-142, 124-140.
561 Rahardjo, H., Satyanaga, A., Leong, E.C., Ng, Y.S., Foo, M.D., Wang, C.L. 2007. Slope
562 Failures in Singapore due to Rainfall. Proceedings of 10th Australia New Zealand

563 Conference on Geomechanics “Common Ground”. Brisbane, Australia, 21-24 October,
564 2, 704 - 709.
565 Romero, S., Pamukcu, S., 1996. Characterization of granular meterial by low strain dynamic
566 excitation and ANN. Geotechnical Special Publication, ASTM-ASCE, 58 (2), 1134-
567 1148.
568 Roslee, R., Jamaluddin, T.A., Talip, M.A., 2012. Intergration of GIS Using GEOSTAtistical
569 INterpolation Techniques (Kriging) (GEOSTAINT-K) in Deterministic Models for
570 Landslide Susceptibility Analysis (LSA) at Kota Kinabalu, Sabah, Malaysia. J.
571 Geography and Geology, 4 (1), 18-32.
572 Satyanaga, A. and Rahardjo, H. 2019. Unsaturated Shear Strength of Soil with Bimodal Soil-
573 water Characteristic Curve. Geotechnique. 69 (9), pp. 828-832.
574 Satyanaga, A., Zhai, Q., Rahardjo, H. 2017. Estimation of Unimodal Water Characteristic
575 Curve for Gap-graded Soil. Soils and Foundations, 5 (5), 789-801.
576 Shahin, M.A., Jaksa, M.B., Maier, H.R., 2000. Predicting the settlement of shallow foundations
577 on cohesionless soils using back-propagation neural networks. Research Report No. R
578 167, The University of Adelaide, Adelaide.
579 Shahin, M.A., Jaksa, M.B., Maier, H.R., 2001. Artificial neural network applications in
580 geotechnical engineering. Australian geomechanics 36 (1), 49-62.
581 Sivakugan, N., Eckersley, J.D., and Li, H.. 1998. Settlement predictions using neural networks.
582 Australian Civil Engineering Transactions, CE40, 49-52.
583 U.S. Army Corps of Engineers, 2003. Engineering and Design SLOPE STABILITY. Engineer
584 Manual. No. 1110-2-1902.
585 Zhai, Q., Rahardjo, H. and Satyanaga, A. 2018. A pore-size distribution function based method
586 for estimation of hydraulic properties of sandy soils. Engineering Geology, 246, 288-
587 292.

588 Zhai, Q., H. Rahardjo, A. Satyanaga, and Priono. 2017. Effect of bimodal soil-water
589 characteristic curve on the estimation of permeability function. Engineering Geology.
590 230, pp. 142-151.